DOI: 10.21062/mft.2024.063 http://www.journalmt.com

The Impact of Pre-Existing Surface Texture on Laser Cladding of 316L Cladding

Chen Ma (0000-0002-4884-235X), Weilong Du (0009-0006-2698-7992), Zice Yu (0009-0001-9279-7197), Zihao Zhang (0009-0007-9868-8972), Changlong Zhao (0000-0001-7778-3494)
College of mechanical and vehicle engineering, Changchun University, Changchun 130022. China. E-mail: mac@ccu.edu.cn

Laser cladding technology, a novel surface modification technique, is widely employed in tasks such as metal surface strengthening and repair. However, the quality post-cladding often falls short of usage requirements, harbouring defects like cracks and pores. In pursuit of a crack-free cladding method, surface texture technology is integrated with laser cladding technology to establish a multi-field coupled numerical simulation model. This model investigates the temperature, stress, and fluid fields during laser cladding with and without texture, aiming to identify the optimal cladding parameters. The results indicate that the optimal cladding parameters are a laser power of 1200 W, a scanning speed of 7 mm.s^{-1}, and a spot radius of 2 mm. In comparison with cladding without texture, the minimum temperature has increased by approximately 50 %, while the peak temperature has remained almost unchanged. The maximum residual stress of the cladding layer without texture is 369.46 MPa, whereas that of the cladding layer with pre-set texture is 338.46 MPa, representing a reduction of approximately 8.39 %. The bottom of the cladding layer has decreased by about 29.1 %, effectively enhancing the mechanical properties at the metallurgical bond of the cladding layer. The pre-set texture induces a decreasing trend in the flow velocity inside the molten pool, eliminating the double-vortex effect, resulting in a more uniform temperature distribution within the molten pool, consequently reducing the residual stress of the cladding layer. This paper employs multi-field coupled numerical simulation technology to monitor the internal state of the molten pool, offering insights for enhancing the quality of the cladding layer in subsequent endeavours.

Keywords: Laser cladding, Surface texture, Multi-field coupled, Residual stress

1 Introduction

Laser cladding technology is an advanced method for material surface improvement and manufacturing. It employs high-energy laser beams to rapidly melt powder, resulting in the solidification of a coating layer on the workpiece surface. This process facilitates precise modification, repair, and manufacturing of workpiece surfaces. Laser cladding technology is widely utilized across various sectors, including aerospace, automotive, mold manufacturing, and medical devices [1-4]. However, this technology has drawbacks including residual stress and deformation, porosity and defects, and relatively high surface roughness [5-7], which limit its development and widespread application in practical scenarios. Overcoming these limitations requires further research and technological improvements to enhance its quality and reliability, better meeting the demands of the engineering sector for high-performance materials.

Researchers have enhanced the surface quality, residual stress, porosity, and surface roughness of laser cladding layers by adjusting processing parameters and introducing auxiliary processing techniques, thereby driving the advancement and utilization of this technology [8-10]. Dara Moazami Goodarzi et al. [11] conducted a study on the relationship between laser cladding process parameters and the geometric structure of cladding layers. Their findings revealed that laser power and cladding speed are the primary parameters governing the width of the cladding layer, while powder feeding speed and cladding speed primarily influence the side angle of the cladding layer. Ayan Bhowmik et al. [12] applied varying laser powers to AI7075 substrates to examine the microstructure of the cladding layer and substrate. Their findings indicated that regardless of the laser power applied, three distinct regions could be identified: the columnar crystal primary zone, the aluminum-silicon eutectic zone, and the non-equilibrium three-phase zone. Qi K et al. [13] applied a magnetic field during the preparation of Co-based cladding layers on 42CrMn substrates. Their findings demonstrated that the magnetic field could enhance the uniformity of element distribution and reduce element segregation. Additionally, the magnetostrictive effect reduced thermal stress during the cladding process, thereby decreasing the sensitivity of cladding layer cracking.

With the accessibility of microfabrication techniques, surface texturing technology has significantly contributed to the flourishing development of tribology in recent years. Many scholars have analyzed the application effects and developmental potential of surface texturing in various aspects, such as friction reduction, lubrication resistance reduction, and corrosion prevention on friction surfaces. The study by He Yang et al. [14] demonstrated that suitable mesh-like textured surface structures can effectively facilitate the formation of lubricating water films on friction surfaces, thereby enhancing the frictional wear performance of bearings. Wang Baomin et al. [15] transformed traditional regular textures into asymmetric textures. The influence of variations in flow field velocity and direction, along with the generation of double vortices at the exit of textured pits, resulted in higher wall pressures at different H values compared to symmetrical textures and non-textured conditions. The highest load capacity and minimum friction coefficient were observed when H=0.25. Furthermore, numerous scholars have pre-set surface textures on cutting tools to enhance their longevity. ARULKIRUBAKARAN et al. [16] employed a combination of simulation and experimentation to fabricate surface textures of various morphologies on WC cutting tools and simulated them using Deform 3D software. The non-textured tool exhibited a chip contact length of 1.3 mm; the parallel groove tool had a chip contact length of 1.18 mm, resulting in a 12 % to 14 % reduction in contact area; the intersecting groove tool had a chip contact length of 0.732 μm, reducing the contact area by 52 %; and the perpendicular groove tool had a chip contact length of 0.642 μm, reducing the contact area by 65 % to 75 %. Li, J et al. [17] utilized lasers to construct biomimetic textures on aluminum alloy substrates, creating special hydrophobic aluminum alloy surfaces through nanocoating technology. The surface properties of the specimens were analyzed using scanning electron microscopy, surface profilometry, and contact angle measurement instruments. The results demonstrated the significant role of biomimetic textures and SAMs in preparing superhydrophobic surfaces.

This paper investigates the impact of surface texturing technology on residual stresses in laser cladding layers by combining surface texturing technology with laser cladding technology using numerical simulation on 316L stainless steel. An orthogonal experimental design is adopted to provide a theoretical foundation for subsequent laser cladding experiments.

2 Numerical simulation

2.1 Material Selection

For this numerical simulation, both the substrate and powder are chosen to be 316L stainless steel, with their chemical compositions listed in Table 1. The thermal properties of 316L stainless steel with temperature variation are computed using the incremental method in JMatPro software and then imported into ANSYS finite element analysis software for numerical simulation. To visually observe the changes in various thermal properties with temperature more clearly, the data are imported into Origin software for plotting, as illustrated in Fig. 1.

Tab. 1 *Composed of 316L stainless steel elements*

Element	Fe	Cr	Mn	Mo	Ni	Si	C
Mass fraction (wg. %)	64.447	17.3	1.74	2.66	13.1	0.73	0.023

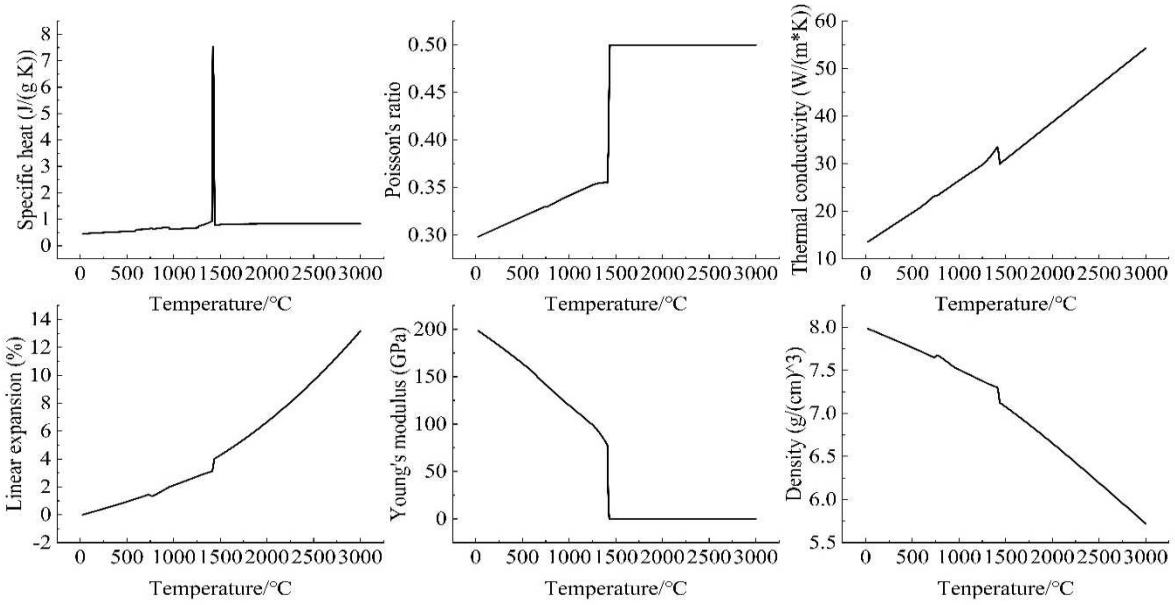

Fig. 1 *Thermophysical properties of 316L stainless steel*

2.2 Multi-field coupled numerical simulation technology

The multi-field coupled numerical simulation technology is an advanced technique that integrates different physical fields for simulation and analysis [18-20]. Through multi-field coupled numerical simulation, more accurate simulations of real situations, including the interactive effects between different physical fields, can enhance the accuracy and reliability of simulation results [21]. This paper couples the temperature field, stress field, and fluid field to numerically simulate the laser cladding process, allowing for a more comprehensive analysis and evaluation of the laser cladding process. To unveil the mechanism through which surface texturing technology impacts the performance of the cladding layer, the laws of multi-field coupling interactions are depicted in Fig. 2.

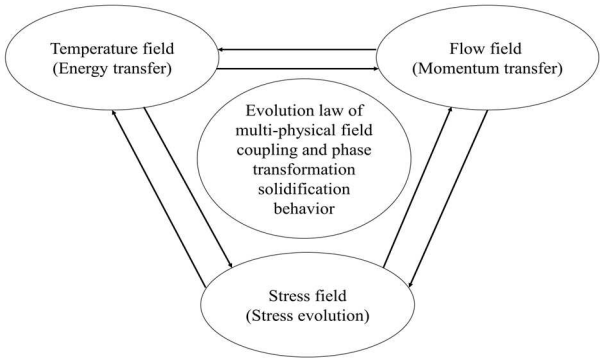

Fig. 2 *Multi-field coupling interaction law of laser cladding*

2.3 The overall governing equation of the laser cladding process

The overall governing equation of the laser cladding process is [22, 23]:

$$\frac{\partial \rho}{\partial t}+\nabla\cdot(\rho v)=0 \tag{1}$$

$$\rho\left[\frac{\partial v}{\partial t}+(v\cdot\nabla)v\right]=\nabla\cdot\left[-pI+\mu\left(\nabla v+(\nabla v)^{T}\right)-\frac{2\mu}{3}(\nabla\cdot v)I\right]-K_0\frac{(1-f_l)^2}{f_l^3+B}v \tag{2}$$

$$\rho C_p\frac{\partial T}{\partial t}+\rho C_p v\cdot\nabla T=\nabla\cdot(k\nabla T)-\frac{\partial H}{\partial t}-\rho v\cdot\nabla H \tag{3}$$

$$\rho\frac{\partial \xi^2}{\partial t^2}=\nabla\cdot S+FV \tag{4}$$

Where:
ρ …Density,
t …Time,
v …The metal flow velocity inside the melt pool,
μ …Fluid dynamic viscosity,
p …Pressure,
T …Temperature,
C_p …Specific heat capacity,
k …Thermal conductivity,
ξ …Displacement vector,
F …Constraint force,
S …Total displacement.

Equation (1) represents the continuity equation, while equation (2) represents the Navier-Stokes momentum equation, where K_0 is a constant determined by the porous morphology, and B is an infinitesimal parameter to avoid division by zero. Equation (3) corresponds to the energy equation, with H representing the metal melting enthalpy, denoted as $\Delta H = Lf_l$, and f_l indicating the liquid mass fraction, represented as:

$$f_l=\begin{cases}1, T>T_l\\ \dfrac{T-T_S}{T_L-T_S}, T_S\le T\le T_l\\ 0, T<T_S\end{cases} \tag{5}$$

In the equation, subscripts S and l denote the solid and liquid phases respectively, with equation (4) denoting the stress equation.

2.4 Heat source selection

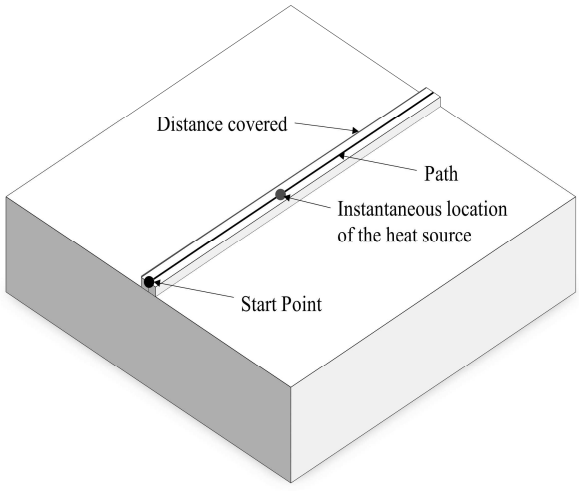

Fig. 3 *Diagram illustrating the principle of heat source application*

The heat source for laser cladding numerical simulation in this paper is selected using the Moving Heat plugin in ANSYS Workbench. The heat source equation defined by this plugin is as follows.

$$q = C_2 e^{-\frac{\left[(x-x_0)^2+(y-y_0)^2+(z-z_0)^2\right]}{C_1^2}} \quad (6)$$

Where:

q …The heat flux,

C_1…The spot radius,

C_2…The laser power,

(x_0, y_0, z_0)…The instantaneous position of the heat source center.

The principle of heat source application by the Moving Heat plugin is illustrated in Fig. 3.

2.5 The finite element model is established

Assumptions for modeling the laser cladding process are as follows:

- (1) Metal flow inside the melt pool is assumed to be laminar and the fluid is assumed to be incompressible Newtonian.
- (2) It is assumed that the energy of the laser beam within the spot follows a Gaussian distribution and the power remains constant.
- (3) The material is assumed to be isotropic.
- (4) It is assumed that the concentration of powder flow follows a Gaussian distribution, and the powder dropped into the melt pool melts immediately.
- (5) The clad material is assumed to obey the Von Mises yield criterion.

The model is created using Solid Works 3D software. The dimensions of the substrate model are 50mm×50mm×10mm, and the cladding layer model dimensions are 2 mm×50 mm×1 mm. The surface texture is defined as a grooved texture with dimensions of 2 mm×50 mm×0.8 mm. The model is meshed to improve both calculation accuracy and speed. Densification of the cladding layer mesh and sparsification of the substrate mesh are performed to achieve this goal. This not only enhances calculation speed but also ensures calculation accuracy, as depicted in Fig. 4. The convective heat transfer coefficient is set to a non-linear convective heat transfer coefficient. A non-linear convective heat transfer coefficient with metallic contact is employed for the contact surface beneath the substrate, while the remaining surface coefficients are set to non-linear convective heat transfer coefficients with air.

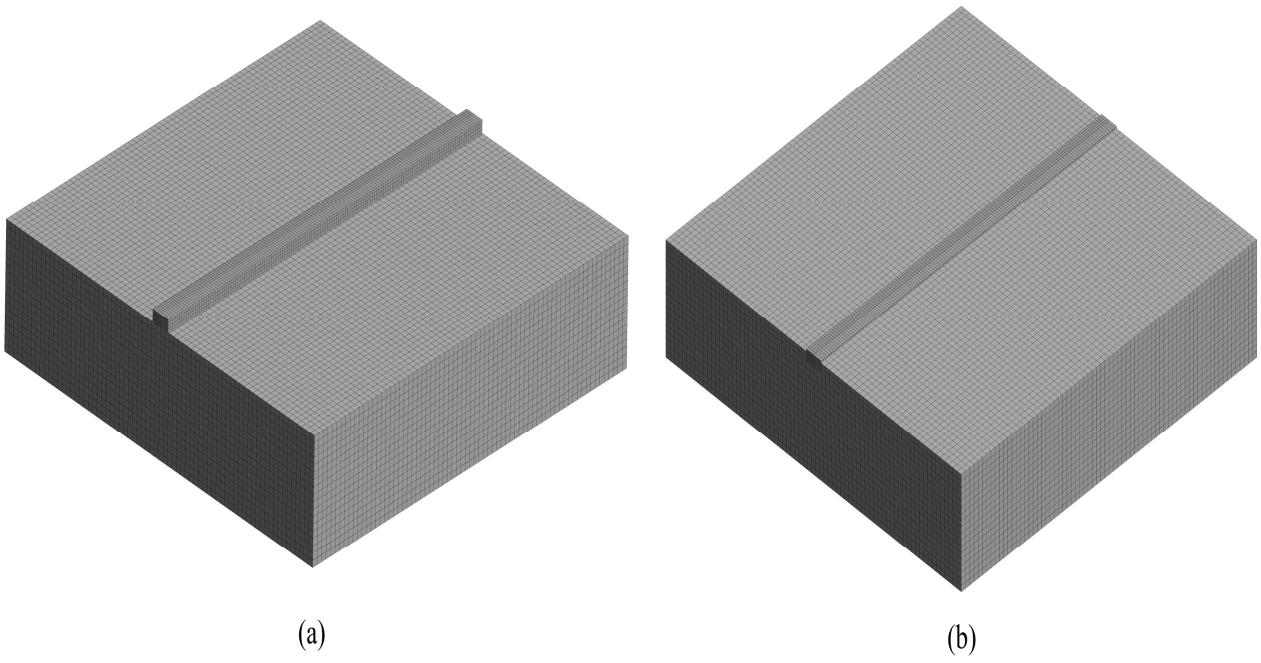

Fig. 4 *(a) Mesh division without texture (b) Mesh division with preset texture*

2.6 Design of numerical simulation experiment scheme

Based on preliminary preparations and relevant literature, laser powers of 600 W, 800 W, 1000 W, 1200 W, and 1400 W, and scanning speeds of 1 mm.sec^{-1}, 2 mm.sec^{-1}, 3 mm.sec^{-1}, 4 mm.sec^{-1}, and 5 mm.sec^{-1} are selected. Since the selection of surface texture morphology depends on the size of the cladding layer, a spot radius of 1mm is chosen. The experimental scheme is designed as shown in Table 2.

Tab. 2 *Numerical simulation experimental setup*

No.	Laser power(W)	Scanning velocity (mm.sec^{-1})	Spot radius(mm)
1	600	1	1
2	600	2	1
3	600	3	1
4	600	4	1
5	600	5	1
6	800	1	1
7	800	2	1
8	800	3	1
9	800	4	1
10	800	5	1
11	1000	1	1
12	1000	2	1
13	1000	3	1
14	1000	4	1
15	1000	5	1
16	1200	1	1
17	1200	2	1
18	1200	3	1
19	1200	4	1
20	1200	5	1
21	1400	1	1
22	1400	2	1
23	1400	3	1
24	1400	4	1
25	1400	5	1

3 Analysis of results

3.1 Analysis of the temperature field results

Laser cladding, a rapid prototyping technology, utilizes a high-power laser beam to melt powder materials and deposit them onto the surface of the substrate, forming parts of the desired shape [24-27]. Achieving high-quality cladding layers requires precise control of the temperature field during the laser cladding process. Laser cladding temperature field simulations with and without texture under different parameters were performed using ANSYS Workbench software, and the simulation results are depicted in Fig. 5.

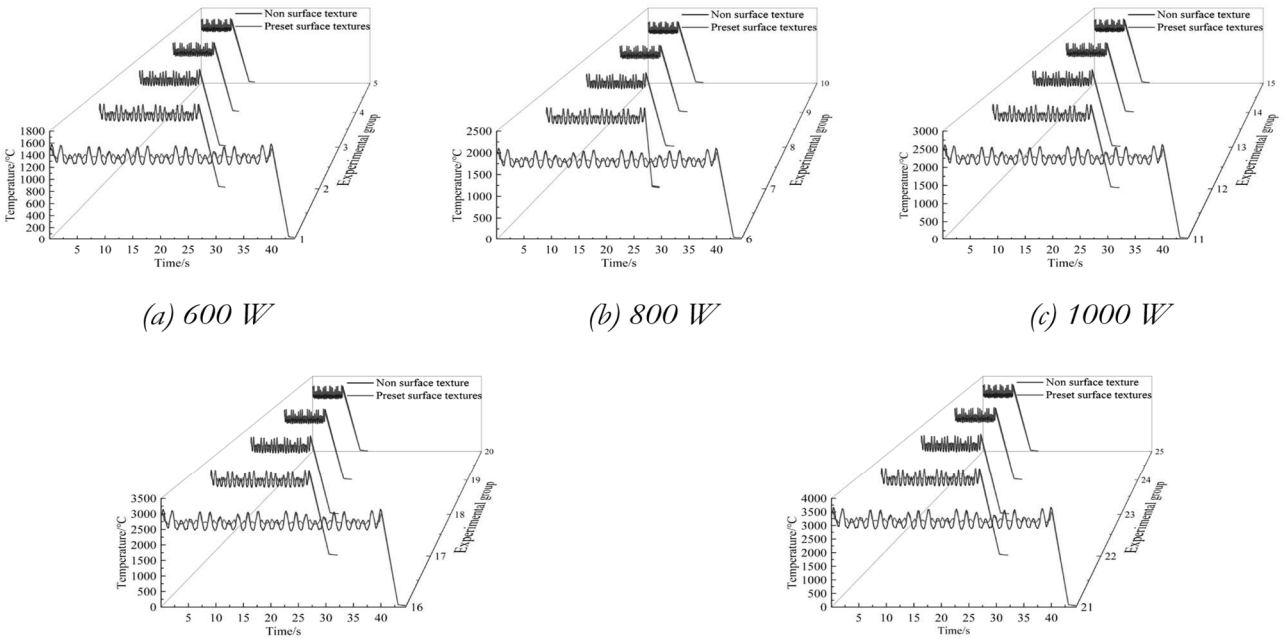

(a) 600 W *(b) 800 W* *(c) 1000 W*

(d) 1200 W *(e) 1400 W*

Fig. 5 *Simulation results of the temperature field under different cladding parameters*

Fig. 5 illustrates the thermal cycle curves under various cladding parameters. In the figure, the blue curve represents the thermal cycle curve without texture, and the red curve represents the thermal cycle curve with pre-set texture. Subfigure (a) maintains a constant laser power of 600 W, with scanning speeds ranging from 1 mm.sec^{-1} to 5 mm.sec^{-1}. The Z-axis in subfigure (a) corresponds to experimental groups 1-5 in the experimental design, while subfigures (b), (c), (d), and (e) vary the laser power, with other settings identical to those in subfigure (a). Observing Fig. 5 reveals that, with a constant scanning speed, the peak temperature in the thermal cycle curve increases with the rising laser power, indicating a positive correlation between the peak temperature and laser power; similarly, at a constant laser power, the peak temperature decreases with the increasing scanning speed, showing a negative correlation between the peak temperature and scanning speed.

Under identical cladding conditions, the minimum temperature during the cladding process with preset surface texture increases by approximately 50% compared to that without texture, while the peak temperature remains virtually unchanged. Given that the laser power and scanning speed are constant, this revision clarifies the relationship between laser energy and temperature change due to the surface texture, improving clarity and coherence.

3.2 Analysis of the stress field results

Laser cladding is an emerging metal manufacturing process capable of producing high-strength, high-performance metal components. However, it also results in significant residual stress. By conducting laser cladding stress field simulations using ANSYS Workbench, it is possible to predict the stress distribution within the cladding layer. Therefore, stress field simulations for laser cladding with and without texture under different parameters were conducted using ANSYS Workbench software, and the simulation results were extracted, as shown in Fig. 6.

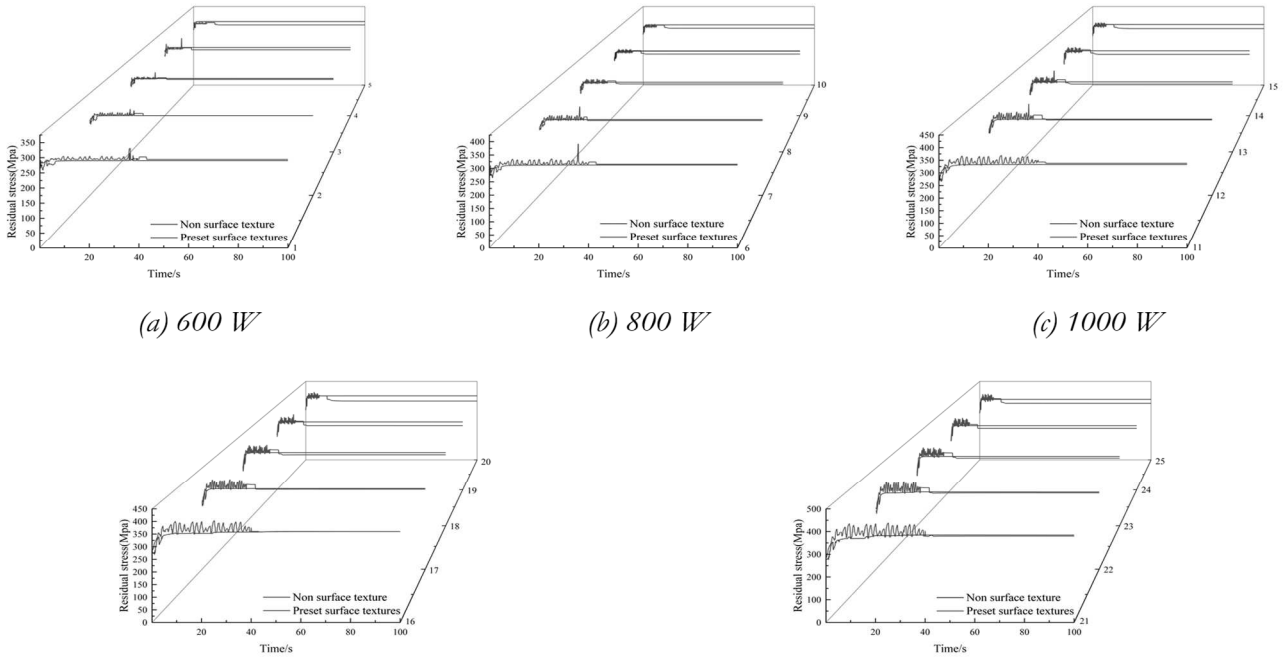

(a) 600 W *(b) 800 W* *(c) 1000 W*

(d) 1200 W *(e) 1400 W*

***Fig. 6** Simulation results of stress fields under different cladding parameters*

Fig. 6 illustrates the residual stress curves under different cladding parameters. The blue curve represents the residual stress curve without texture, while the red curve represents the residual stress curve with pre-set texture. Subfigure (a) maintains a constant laser power of 600W, with scanning speeds of 1 mm.sec^{-1}, 2 mm.sec^{-1}, 3 mm.sec^{-1}, 4 mm.sec^{-1}, and 5 mm.sec^{-1}, corresponding to experimental groups 1 to 5 on the Z-axis. Subfigures (b), (c), (d), and (e) vary the laser power, with other settings consistent with subfigure (a). Observing from Figure 6(a) to (e), it can be seen that both residual stress curves with and without texture exhibit unstable alternating thermal stresses. Unstable alternating thermal stresses without texture mainly occur at the beginning of cladding, while those with pre-set texture persist throughout the cladding process. Some studies have indicated that unstable alternating thermal stresses can enhance the mechanical properties of material surfaces, improve wear resistance, and enhance cladding layer quality. In line with the findings of this study, the presence of surface texture leads to the generation of unstable alternating

thermal stresses during the cladding process. Residual stresses are generally lower than those without texture under most cladding parameters, such as experimental groups 4, 5, 8, 9, and 10, with only a few cases showing minimal differences from the residual stresses without texture, such as experimental groups 1, 2, 6, and 11. Additionally, the results indicate that when the scanning speed is low, the difference in residual stress between pre-set texture and no texture is minimal, whereas at higher scanning speeds, the difference in residual stress between pre-set texture and no texture is significant.

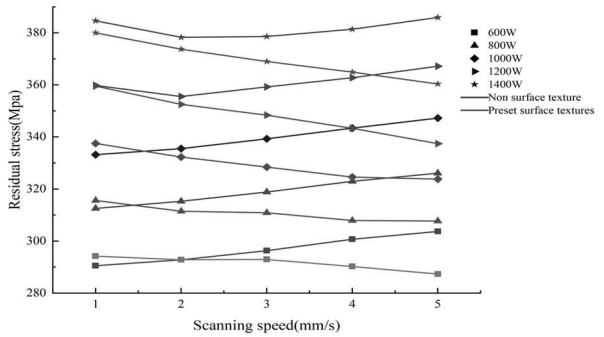

Fig. 7 *Comparison chart of residual stresses for each group*

In Fig. 7, blue represents the non-textured experimental group, while red represents the pre-textured experimental group, with different symbols used to denote varying powers. Observation from Fig. 7 reveals that in the non-textured experimental group, when the laser power remains constant, the residual stress of the clad layer gradually increases with the rise in scanning speed; similarly, with constant scanning speed, the residual stress of the clad layer increases gradually with higher laser power, demonstrating a positive correlation between residual stress and both laser power and scanning speed. In the pre-textured experimental group, it is observed that when the laser power remains constant, the residual stress of the clad layer gradually decreases with increasing scanning speed; conversely, with constant scanning speed, the residual stress of the clad layer gradually increases with higher laser power, suggesting a positive correlation with laser power but a negative correlation with scanning speed. In the proposed experimental setup, the pre-textured group exhibits a maximum reduction in residual stress of 8.09% compared to the non-textured group, with laser power set at 1200 W, scanning speed at 5 mm.sec^{-1}, and spot radius at 1mm. Combining Figures 6 and 7, it is noted that with constant laser power, the residual stress of the pre-textured clad layer decreases as scanning speed increases. To explore the relationship between pre-textured surfaces and scanning speed, a constant laser power of 1200 W and scanning speeds ranging from 1 mm.sec^{-1} to 10 mm.sec^{-1} were selected for numerical simulation of textured and non-textured laser cladding.

3.3 The influence of scanning speed on residual stress in relation to texture

Laser cladding is a process whereby the material surface is irradiated by laser, rapidly melting and solidifying to form a new material layer. During this process, the energy from the laser induces localized expansion and contraction of the material, thereby generating residual stress. The scanning speed is a critical parameter in the laser cladding process, determining both the size of the laser irradiation area and the melting time. In practical applications, the relationship between scanning speed and residual stress is not simply linear. Fig. 7 clearly shows that the residual stress without texture increases as the scanning speed increases, whereas the residual stress with pre-set texture decreases with increasing scanning speed. With a laser power of 1200 W, scanning speeds ranging from 1 mm.sec^{-1} to 10mm.sec^{-1}, and a spot radius of 1mm, numerical simulations of residual stress for laser cladding with and without texture are presented in Figure 8. Residual stress comparison is depicted in Fig. 9, and the percentage decrease in residual stress with and without texture is illustrated in Fig. 10.

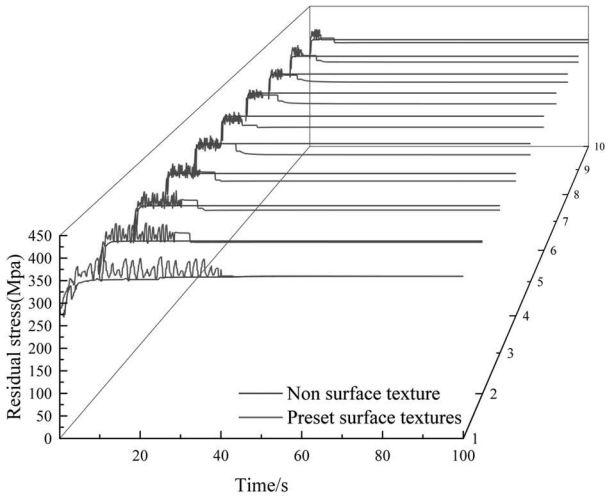

Fig. 8 *Simulation results of the stress field*

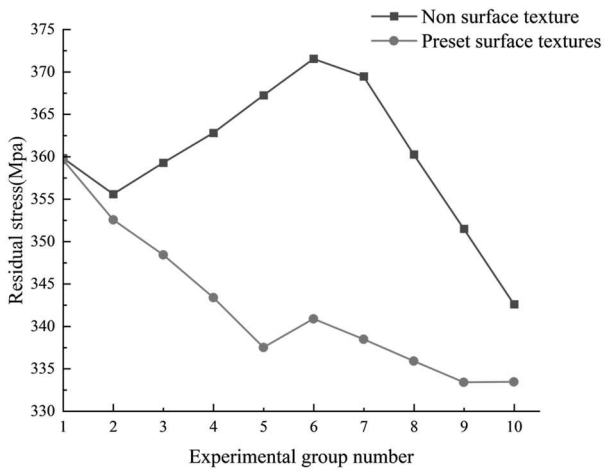

Fig. 9 *Comparison chart of residual stress*

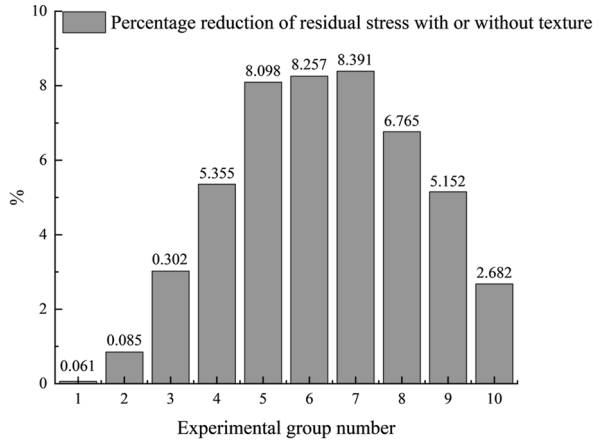

Fig. 10 *Percentage decrease in residual stress*

From Fig. 8, it is observed that with a constant laser power of 1200 W, the scanning speed gradually increases from 1 mm.sec^{-1} to 10 mm.sec^{-1}. Pre-set texture consistently enhances the unstable alternating thermal stress during scanning speeds ranging from 1 mm.sec^{-1} to 10 mm.sec^{-1}. In Fig. 9, the residual stress curves of laser cladding with and without texture exhibit a trend of initially decreasing, then increasing, and then decreasing again as the scanning speed increases. However, the residual stress with pre-set texture is generally lower than that without texture. At a scanning speed of 7 mm.sec^{-1}, the residual stress without texture is 369.46 MPa, while the residual stress with pre-set texture is 338.46 MPa, indicating a reduction in residual stress of approximately 8.39 %. Fig. 10 illustrates that the percentage decrease in residual stress with and without texture initially increases and then decreases with increasing scanning speed. A comprehensive analysis of Figures 8, 9, and 10 indicates that pre-set texture effectively reduces residual stress in laser cladding, enhancing the unstable alternating thermal stress during the process. Within a certain range of cladding parameters, pre-set surface texture can effectively improve the quality of the clad layer and reduce residual stress. Residual stress contour maps of laser cladding layers with and without texture for Experiment Group 7 are depicted in Fig. 11.

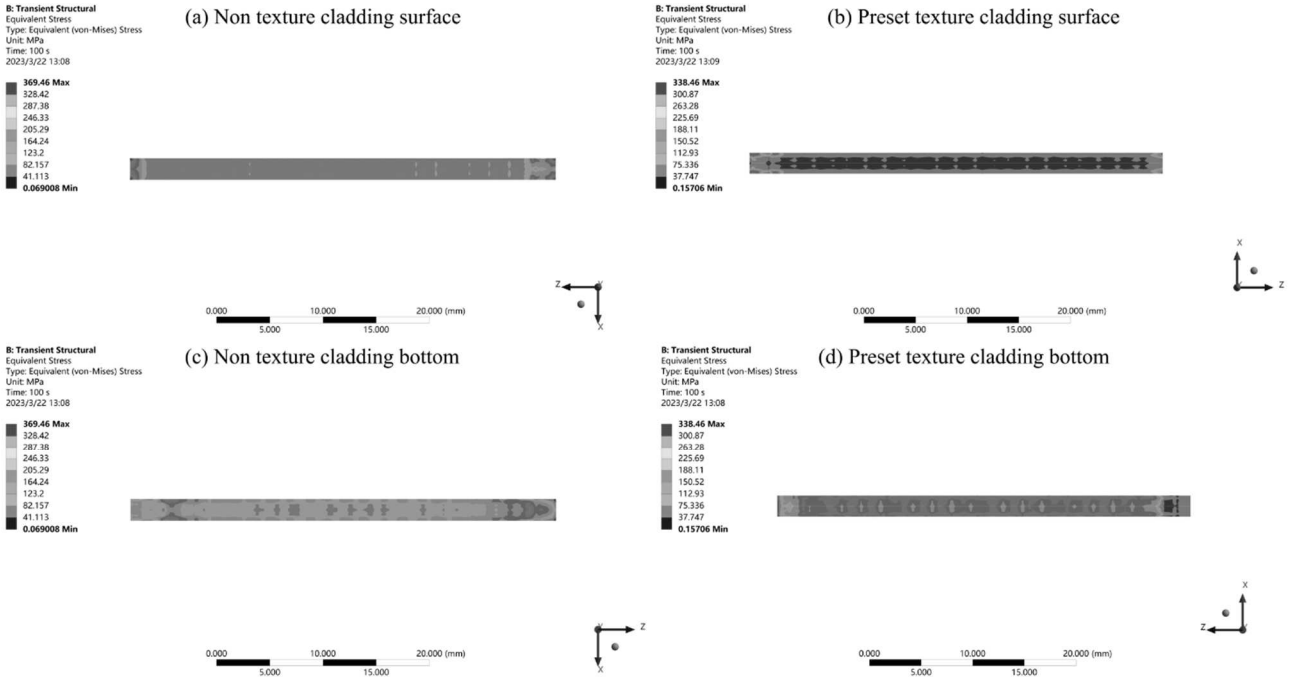

Fig. 11 *Contour maps of residual stress in laser cladding layers with and without texture*

In Fig. 11, (a) depicts the surface of the laser cladding layer without texture, with residual stress values ranging mainly from 246.33 MPa to 328.42 MPa, (b) depicts the surface of the laser cladding layer with pre-set texture, with residual stress values ranging mainly from 263.28 MPa to 338.46 MPa, (c) illustrates the bottom surface of the laser cladding layer without texture, with residual stress values ranging mainly from 246.33 MPa to 328.42 MPa, (d) illustrates the bottom surface of the laser cladding layer with pre-set texture, with residual stress values ranging mainly from 150.52 MPa to 263.28 MPa. Fig. 11 clearly demonstrates that the residual stress on the bottom surface of the laser cladding layer with pre-set texture is relatively low. However, the difference between the surface of the cladding layer with and without texture is minimal, and in some cases, it is even higher than that of the cladding layer without texture. Therefore, in order to investigate the distribution of residual stresses in the two types of laser cladding layers, the stresses in the X, Y and Z directions of the laser cladding layers were extracted, respectively, and the sampling schematic is

shown in Fig. 12, and the results are shown in Fig. 13. The residual stress curves in the X direction of the laser cladding layers with and without texture are essentially symmetric on both sides, and their trends are generally consistent. However, the residual stress in the X direction of the laser cladding layer with pre-set texture is consistently lower than that of the layer without texture. The residual stress in the Y direction of the laser cladding layers with and without texture exhibits a trend of initially increasing and then decreasing. While the residual stress on the surface of the laser cladding layer with pre-set texture is higher than that of the layer without texture, the difference between them is relatively small. Since the surface of the workpiece after laser cladding requires mechanical processing before being used, the residual stress on the cladding layer surface has minimal impact on the workpiece. The bottom of the laser cladding layer with pre-set texture is reduced by approximately 29.1 % compared to that without texture, thereby effectively improving the mechanical properties at the metallurgical bond interface of the cladding layer. Residual stress curves in the Z direction all exhibit significant residual stress at the beginning and end of the cladding, with both positions of the laser cladding layer with pre-set texture being greater than those without texture. This is attributed to the grooved texture prepared in this study, where both positions during melting are at the edge of the workpiece, potentially leading to droplet spattering and consequently significant residual stress. Apart from the aforementioned two positions, residual stress in the Z direction of the laser cladding layer with pre-set texture is lower than that without texture, further validating the effectiveness of pre-set texture technology in reducing residual stress in the cladding layer and enhancing its quality.

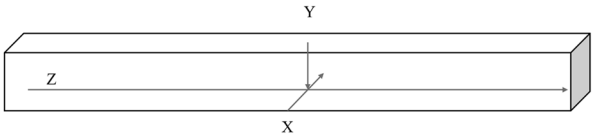

Fig. 12 *Schematic diagram showing sampling points in the X, Y, and Z directions of the cladding layer*

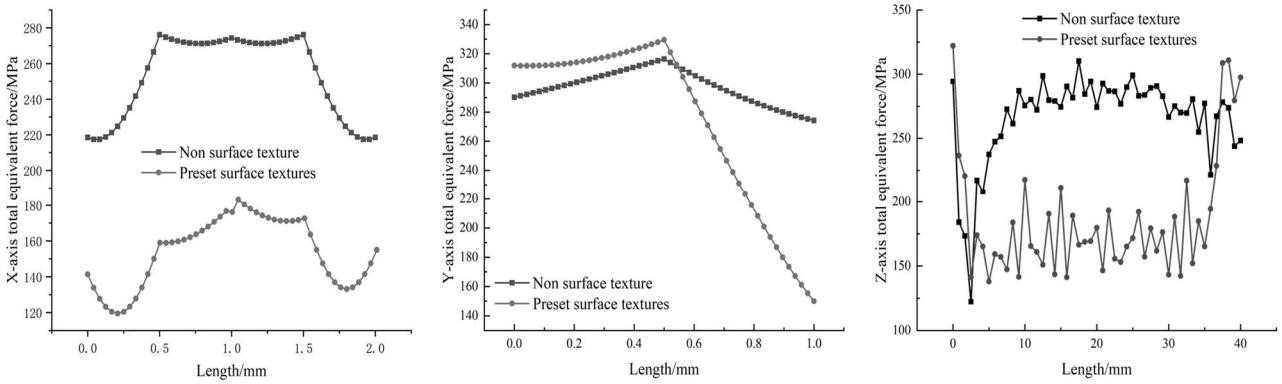

Fig. 13 *Residual stress curves in the X, Y, and Z directions*

4 Analysis of fluid field results

This study utilizes the Volume of Fluid (VOF) model for fluid field simulation, which is grounded on the principles of mass conservation and Navier-Stokes equations. It characterizes the fluid's movement and morphological alterations by tracking the position of the liquid surface and the volume fraction of the liquid phase. The conservation of mass equation describes the rate of mass change in relation to spatial and temporal changes for a fluid. In the Eulerian description, the mass conservation equation is formulated as:

$$\frac{\partial \rho}{\partial t} + \nabla \cdot (\rho u) = 0 \qquad (7)$$

Where:

ρ …The density of the fluid,

u …The velocity vector,

∇ …The divergence operator, which operates on the velocity vector to compute its divergence.

The Navier-Stokes equations constitute the fundamental equations governing fluid motion, encompassing properties such as velocity, density, pressure, viscosity, etc. They are commonly employed to characterize fluid flow and mechanical behavior. The specific expression is as follows:

$$\rho\left(\frac{\partial \rho}{\partial t} + u \cdot \nabla u\right) = -\nabla p + \mu \nabla^2 u + f \qquad (8)$$

Where:

ρ …The fluid density,

u …The velocity vector,

p …Pressure,

μ …The fluid's dynamic viscosity,

∇^2 …The Laplace operator,

f …The external force term.

The left-hand side of the equation represents inertial forces, while the right-hand side comprises three terms: pressure, viscosity, and external forces.

Simulations are performed on the fluid field in laser cladding with and without texture. Velocity vector plots of the clad pools with and without texture are extracted, as illustrated in Fig. 14-18, where blue indicates air and red indicates substrate. Each figure provides a comparison of velocity vectors with and without texture.

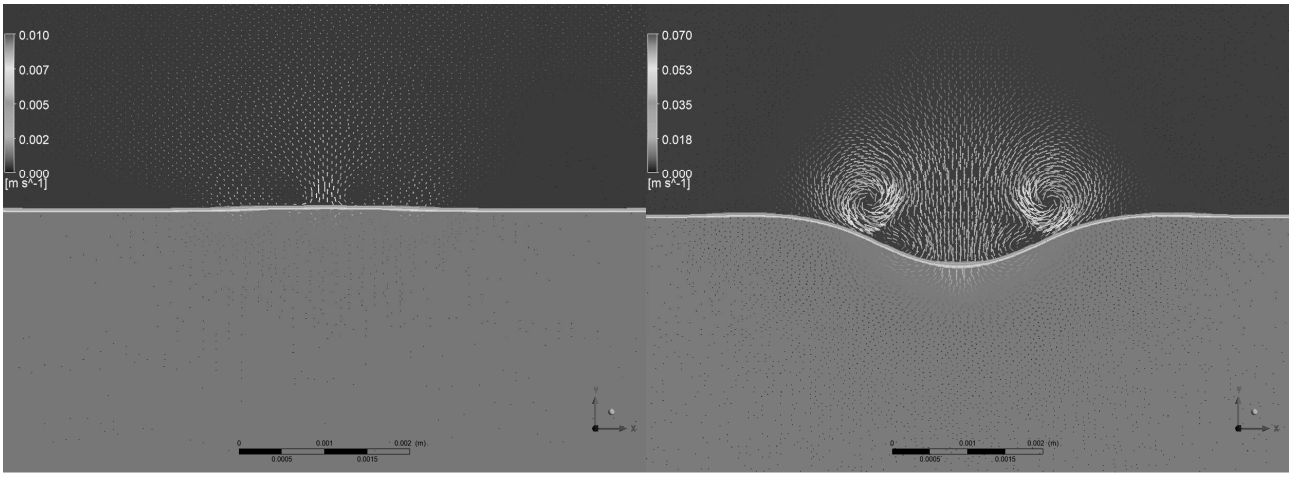

(a) Non surface texture (b) Preset surface textures

Fig. 14 *Velocity vector plots of clad pools with and without texture at 0.01s are displayed*

At 0.01 s, convection appears at the untextured clad pool's air position, reaching a maximum velocity of 0.01 m/s. The internal flow velocity within the pool ranges from 0.002 m/s to 0.005 m/s. Texturing on the substrate surface results in a dual-vortex effect at the air position of the textured clad pool, with a maximum velocity of 0.07 m/s, and internal flow velocities within the pool ranging from 0.018 m/s to 0.035 m/s. Thanks to the good accessibility of the laser, texturing effectively increases the contact area between the laser and the substrate, rapidly elevating temperatures on both sides of the texture to the melting point. A height difference exists between the texture on both sides and the bottom, causing liquid metal on both sides to slide towards the bottom, resulting in significantly higher flow velocities at the beginning of cladding.

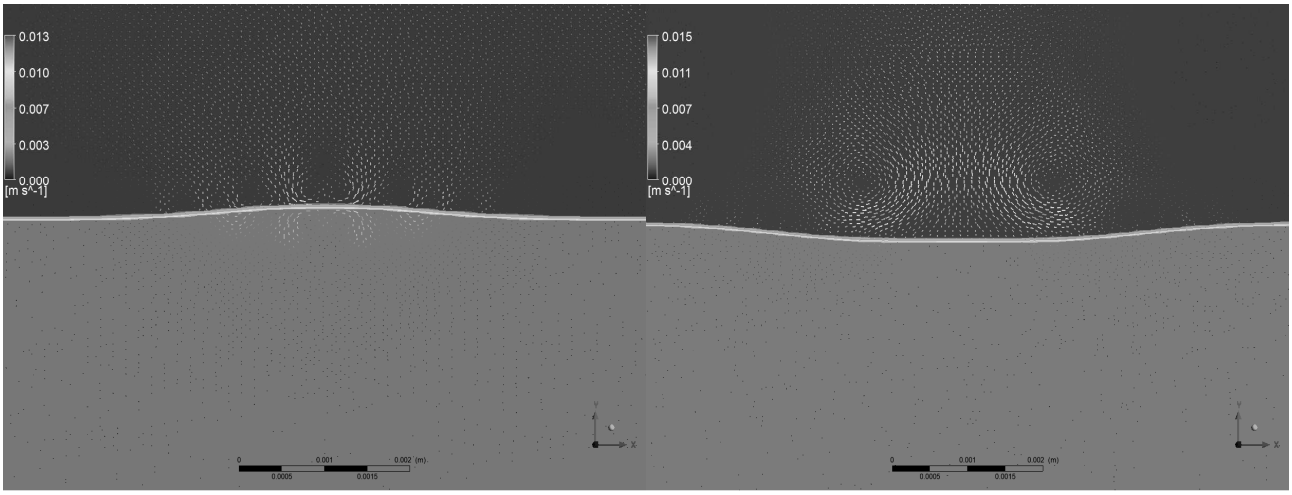

(a) Non surface texture (b) Preset surface textures

Fig. 15 *Velocity vector plots of clad pools with and without texture at 0.05s are displayed*

At 0.05 s, the maximum velocity at the air position of the untextured clad pool increases to 0.013 m/s, while it decreases to 0.015 m/s for the textured clad pool, with a reduction in the dual vortex effect. Observing the velocity vector plots at this time, the textured morphology gradually disappears as the powder is gradually added. At this point, the maximum velocities at the air positions under both cladding methods differ slightly. The reason for the velocity difference observed at 0.01 s is that the presence of texture affects the surface morphology of the substrate, resulting in different locations of air convection occurrence. Untextured cladding acts only on the surface of the substrate, forming natural convection, while textured cladding acts on the bottom of the texture and contacts the sides of the texture, thereby forming the dual

vortex effect. At this time, the internal flow velocity of the untextured clad pool ranges from 0.003 m/s to 0.007 m/s, while that of the textured clad pool ranges from 0 to 0.004 m/s. Compared to the 0.01 s time point, the internal flow velocity of the untextured clad pool gradually increases, while that of the textured clad pool gradually decreases.

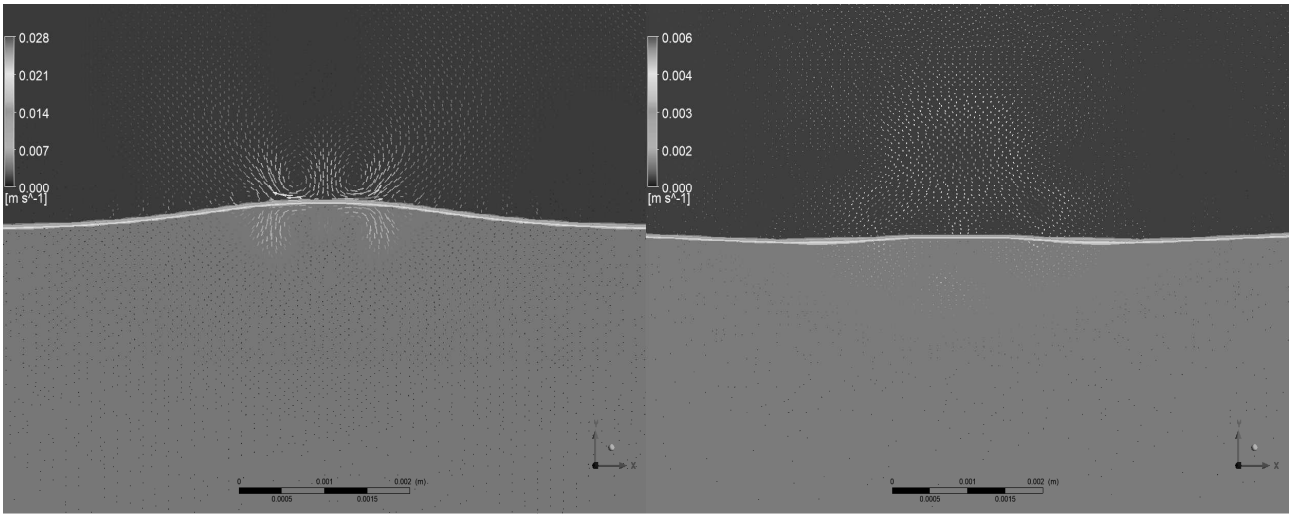

(a) Non surface texture (b) Preset surface textures

Fig. 16 *Velocity vector plots of clad pools with and without texture at 0.10s are displayed*

At 0.10 s, the maximum velocity at the air position of the untextured clad pool is 0.028 m/s, while that of the textured clad pool is 0.006 m/s, with the complete disappearance of the dual vortex effect. At this time, the textured morphology has completely disappeared, similar to the untextured starting point, and there is no dual vortex effect at the air position. The internal flow velocity of the untextured clad pool ranges from 0.014 m/s to 0.021 m/s, while that of the textured clad pool ranges from 0.002 m/s to 0.003 m/s. This is consistent with the trend observed at 0.05 s, where the internal flow velocity of the untextured clad pool gradually increases while that of the textured clad pool gradually decreases.

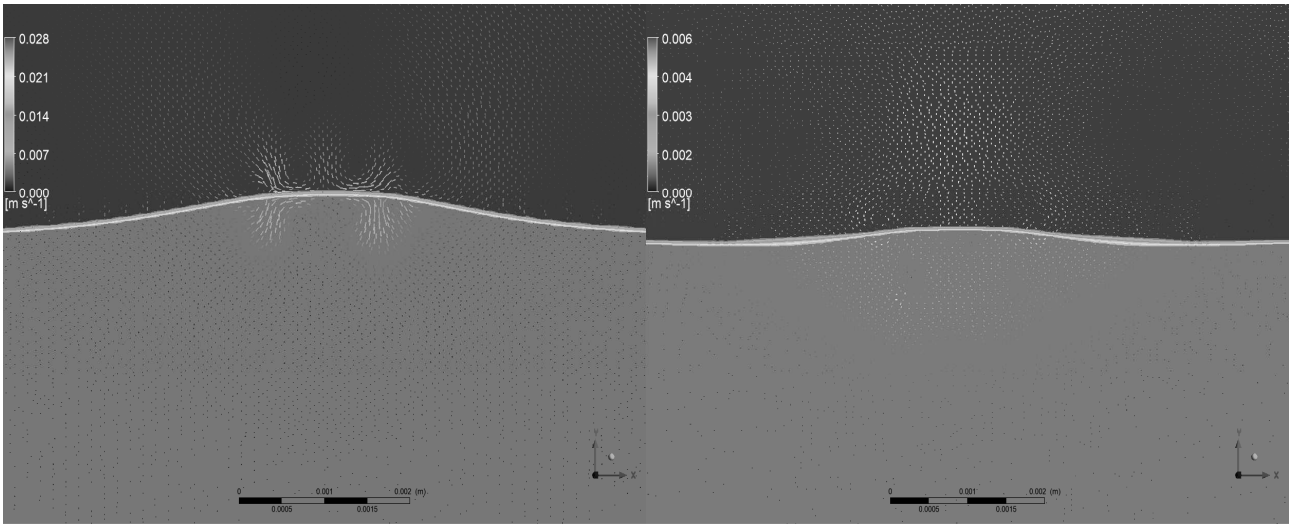

(a) Non surface texture (b) Preset surface textures

Fig. 17 *Velocity vector plots of clad pools with and without texture at 0.15s are displayed*

At 0.15 s, the maximum velocity at the air position of the untextured clad pool is 0.022 m/s, while that of the textured clad pool is 0.006 m/s. At this time, the air velocity in the untextured pool shows a decreasing trend compared to 0.10 s, while the air velocity in the textured pool remains essentially unchanged. The internal flow velocity of the untextured clad pool ranges from 0.014 m/s to 0.021 m/s, while that of the textured clad pool ranges from 0.02 m/s to 0.03 m/s. Compared to 0.10 s, the internal flow velocity of the untextured clad pool remains essentially unchanged, while that of the textured surface continues to decrease.

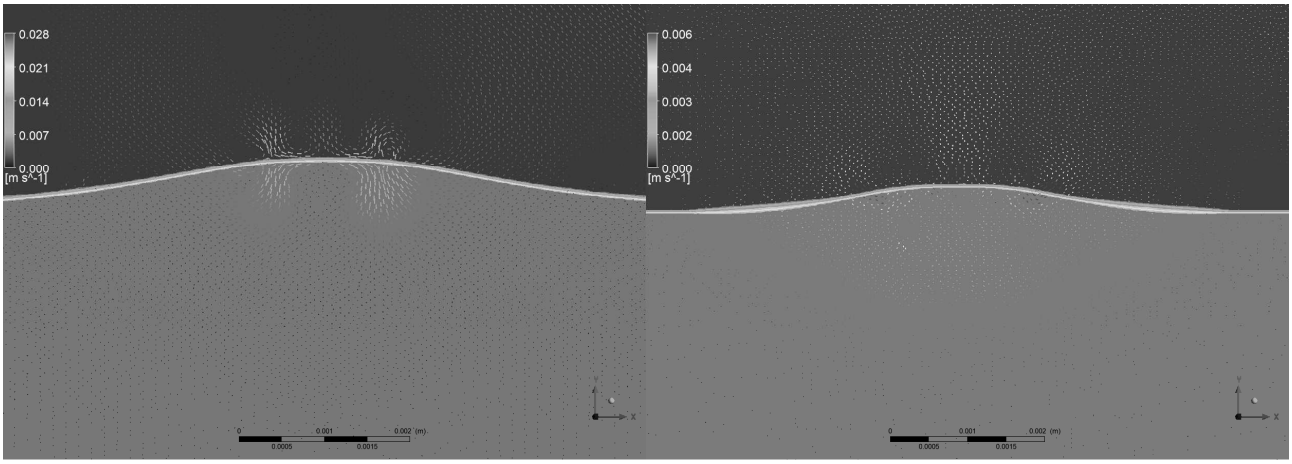

(a) Non surface texture (b) Preset surface textures

Fig. 18 *Velocity vector plots of clad pools with and without texture at 0.20s are displayed*

At 0.20 s, compared with the 0.15 s moment, the airflow velocity at both the air position and the melt pool position remains essentially constant during the non-textured deposition process. In conclusion, during the formation process of the non-textured melt pool, both the airflow and melt pool velocities exhibit an upward trend, remaining essentially constant in the end, while the pre-textured airflow and melt pool velocities show a downward trend, remaining essentially constant in the end. Through the analysis of internal flow velocity in the melt pool, it is observed that the internal flow velocity of the non-textured melt pool shows an increasing trend with time. Due to the inertia effect of fluid motion, the increase in the flow velocity of liquid metal will lead to the formation of vortex flow inside the liquid metal, which in turn causes an uneven temperature distribution within the melt pool, resulting in a significant temperature gradient, consistent with the numerical simulation results of the temperature field mentioned earlier. The presence of temperature gradients induces convection movements within the melt pool, exacerbating the degree of fluid mixing, leading to more pronounced temperature differences in different positions of the liquid, resulting in larger residual stresses in the cladding layer. Conversely, in the pre-textured melt pool, the internal flow velocity decreases with increasing time, and the reduction in flow velocity within the melt pool prevents the generation of vortex effects. As a result, the temperature distribution within the melt pool becomes uniform, leading to a decrease in temperature gradients and consequently smaller residual stresses in the overlay layer, consistent with the numerical simulation results mentioned earlier.

5 Conclusion

This paper combines laser cladding technology with surface texturing technology, and the conclusions are as follows:

- Based on the temperature field analysis, with constant laser power and scanning speed, the energy output of the laser per unit time remains constant, resulting in minimal variation in the peak temperature within the thermal cycle curve. However, pre-textured surfaces effectively increase the contact area between the laser and the substrate, leading to greater absorption of laser energy within the same time period. Consequently, the minimum temperature in the thermal cycle curve increases by approximately 50%, reducing the temperature gradient during the cladding process.
- Analysis of the stress field indicates that under the optimal cladding parameters, the bottom of the pre-textured cladding layer decreases by approximately 29.1 % compared to the non-textured cladding layer. This effectively enhances the mechanical properties at the metallurgical bond interface of the cladding layer.
- Analysis of the fluid field reveals that the internal flow velocity within the pre-textured melt pool decreases with time. This reduction in flow velocity within the melt pool prevents the generation of vortex effects, resulting in a more uniform temperature distribution within the melt pool. Consequently, the temperature gradient decreases, leading to smaller residual stresses in the formed cladding layer.

Combining surface texturing technology with laser cladding technology can effectively reduce residual

stresses in the cladding layer, offering insights for enhancing the quality and performance of the cladding layer.

Acknowledgement

This work was financially supported by Science and Technology Project of Jilin Provincial Science and Technology Department of China (20240101088JC).

Reference

[1] WU J, ZHU DD, YANG RC, WU SY, HUANG Y, ZHANG YL (2021). Parameters Optimization and Friction and Wear Properties for Laser Cladding Ni60AA Coating on 45 Steel Shaft Surface. *Laser & Optoelectronics Progress*, 58(11).

[2] LI TC, ZHANG LL, CHANG C, WEI L (2018). A Uniform-Gaussian distributed heat source model for analysis of residual stress field of S355 steel T welding. *Advances in Engineering Software*, 126, pp.1-8.

[3] TSENG WC, AOH JN (2013). Simulation study on laser cladding on preplaced powder layer with a tailored laser heat source. *Optics and Laser Technology*, 48, pp.141-52.

[4] ZHAO CL, YANG JB, LI M, ZHAO QX, MA HN, JIA XY, ZHANG HF (2023). Advances in Surface Laser Cladding Remanufacturing of Shaft Parts. *Manufacturing Technology*, 23(4), pp.564-578.

[5] ZHAO CL, YANG JB, LI M, ZHAO QX, MA HN, JIA XY, ZHANG HF (2023). Effect on Surface Properties of H13 Mold Steel Cladding Layer by Scanning Strategy. *Manufacturing Technology*, 23(3), pp.380-390.

[6] MICHNA Š, HREN I, MICHNOVÁ L, LATTNER M (2019). Microstructure Study of the Stainless Steel Layer on AlSi Cast Alloy Prepared by Laser Deposition. *Manufacturing Technology*, 19(4), pp.644-646.

[7] YAMAGUCHI T, HAGINO H (2021). Effects of the ambient oxygen concentration on WC-12Co cermet coatings fabricated by laser cladding. *Optics and Laser Technology*, 139.

[8] HAN X, LI C, YANG YP, GAO X, GAO HX (2021). Experimental research on the influence of ultrasonic vibrations on the laser cladding process of a disc laser. *Surface & Coatings Technology*, 406.

[9] WANG S, ZHENG S, LIU WJ, ZHU XD, ZHOU MA, JIANG H (2021). Optimization of Process Parameters for Laser Cladding Fe35A Alloy on 45 Steel Surface. *Laser & Optoelectronics Progress*, 58(9).

[10] LIU WW, SALEHEEN KM, AL-HAMMADI G, DAAIM M, ABDELRAHMAN A, XUE L (2022). Effect of different laser scanning sequences on temperature field and deformation of laser cladding. *Optical Engineering*, 61(4).

[11] GOODARZI DM, PEKKARINEN J, SALMINEN A (2017). Analysis of laser cladding process parameter influence on the clad bead geometry. *Welding in the World*, 61(5), pp.883-91.

[12] BHOWMIK A, YANG YJ, ZHOU W, CHEW YX, BI GJ (2021). On the heterogeneous cooling rates in laser-clad Al-50Si alloy. *Surface & Coatings Technology,* 408.

[13] QI K, YANG Y, SUN R, HU GF, LU X, LI JD (2021). Effect of magnetic field on crack control of Co-based alloy laser cladding. *Optics and Laser Technology*, 141.

[14] HE YANG, GUO ZHIWEI, WU ZUWEN, YUAN CHENGQING (2021). Effect of Surface Mesh Texture on Friction and Wear Properties of Water-Lubricated Bearings. *Lubrication Engineering*, 46(01), pp.31-37.

[15] WANG BAOMIN, NAN YANG (2022). Influence of Asymmetric Surface Texture on Friction Performance of Journal Bearings. *Lubrication Engineering*, 47(02), pp.1-7.

[16] ARULKIRUBAKARAN D, SENTHILKUMAR V, KUMAWAT V (2016). Effect of micro-textured tools on machining of Ti-6Al-4V alloy: An experimental and numerical approach. *International Journal of Refractory Metals & Hard Materials*, 54, pp.165-177.

[17] LI J, HUANG RM, WANG CL, WU HC, ZHANG Y (2020). Effects of Biomimetic Microtexture and Fluoroalkylsilane Modification on Wettability of 6061 Aluminum Alloy. *China Surface Engineering*, 33(2), pp.29-36.

[18] ZHANG KH, WANG JX, BAN YH, SUN CX, GAO PJ, JIN D (2020). Multi-field Coupling Simulation of Gear: A Review. *Journal of Failure Analysis and Prevention*, 20(4), pp.1323-32.

[19] LI C, ZHANG DC, GAO X, GAO HX, HAN X (2022). Numerical simulation method of the multi-field coupling mechanism for laser cladding 316L powder. *Welding in the World*, 66(3), pp.423-40.

[20] HAN X, LI C, CHEN XX, JIA SL (2022). Numerical simulation and experimental study on

the composite process of submerged arc cladding and laser cladding. *Surface & Coatings Technology*, 439.

[21] YUAN WY, LI RF, CHEN ZH, GU JY, TIAN YT (2021). A comparative study on microstructure and properties of traditional laser cladding and high-speed laser cladding of Ni45 alloy coatings. *Surface & Coatings Technology*, 405.

[22] PI ZQ, QIU CJ, FAN XF (2011). Study of Crack Control for CoNiCrWC Composite Coating by Laser Cladding. *Rare Metal Materials and Engineering*, 40, pp.283-5.

[23] LI XB, LI T, SHI BW, WANG D, ADNAN M, LU HT (2020). The influence of substrate tilt angle on the morphology of laser cladding layer. *Surface & Coatings Technology*, 391.

[24] JING ZJ, XU P, LIU QB, YU C (2023). Residual stress release during laser cladding process: A review. *Journal of Laser Applications*, 35(3).

[25] HU H, IQBAL A, WANG XL, ZHANG HC (2015). Experimental Investigation of Residual Stress Relief Using Pre- and Post-clad Heating in the Laser Cladding Process. *Lasers in Engineering*, 31(1-2), pp.11-27.

[26] ZHANG Q, XU P, ZHA GQ, OUYANG Z, HE DT (2021). Numerical simulations of temperature and stress field of Fe-Mn-Si-Cr-Ni shape memory alloy coating synthesized by laser cladding. *Optik*, 242.

[27] WANG Q, SHI JM, ZHANG LX, TSUTSUMI S, FENG JC, MA NS (2020). Impacts of laser cladding residual stress and material properties of functionally graded layers on titanium alloy sheet. *Additive Manufacturing*, 35.